Original Research

Evaluation of Different Cerebral Mass Lesions by Perfusion-Weighted MR Imaging

Bahattin Hakyemez, MD,[1,2]* Cuneyt Erdogan, MD,[1] Naile Bolca, MD,[1] Nalan Yildirim, MD,[3] Gokhan Gokalp,[1] and Mufit Parlak, MD[1]

Purpose: To investigate the contribution of perfusion-weighted MR imaging (PWI) by using the relative cerebral blood volume (rCBV) ratio in the differential diagnosis of various intracranial space-occupying lesions.

Materials and Methods: This study involved 105 patients with lesions (high-grade glioma ($N = 26$), low-grade glioma ($N = 11$), meningioma ($N = 23$), metastasis ($N = 25$), hemangioblastoma ($N = 6$), pyogenic abscess ($N = 4$), schwannoma ($N = 5$), and lymphoma ($N = 5$)). The patients were examined with a T2*-weighted (T2*W) gradient-echo single-shot EPI sequence. The rCBV ratios of the lesions were obtained by dividing the values obtained from the normal white matter. Statistical analysis was performed with the Mann-Whitney U-test. A P-value less than 0.05 was considered statistically significant.

Results: The rCBV ratio was 5.76 ± 3.35 in high-grade gliomas, 1.69 ± 0.51 in low-grade gliomas, 8.02 ± 3.89 in meningiomas, 5.27 ± 3.22 in metastases, 11.36 ± 4.41 in hemangioblastomas, 0.76 ± 0.12 in abscesses, 1.10 ± 0.32 in lymphomas, and 3.23 ± 0.81 in schwannomas. The rCBV ratios were used to discriminate between 1) high- and low-grade gliomas ($P < 0.001$), 2) hemangioblastomas and metastases ($P < 0.05$), 3) abscesses from high-grade gliomas and metastases ($P < 0.001$), 4) schwannomas and meningiomas ($P < 0.001$), 5) lymphomas from high-grade gliomas and metastases ($P < 0.001$), and 6) typical meningiomas and atypical meningiomas ($P < 0.01$).

Conclusion: rCBV ratios can help discriminate intracranial space-occupying lesions by demonstrating lesion vascularity. It is possible to discriminate between 1) high- and low-grade gliomas, 2) hemangioblastomas and other intracranial posterior fossa masses, 3) abscesses from high-grade gliomas and metastases, 4) schwannomas and meningiomas, 5) lymphomas and high-grade gliomas and metastases, and 6) typical and atypical meningiomas.

Key Words: brain; neoplasm; magnetic resonance; perfusion-weighted; grading
J. Magn. Reson. Imaging 2006;24:817–824.

PERFUSION-WEIGHTED MRI (PWI) provides information about cerebral tissue physiology, in contrast to conventional MR techniques (1). Conventional techniques are adequate for detecting intracranial masses, but cannot be used to grade tumors and discriminate lesions from each other (2). In addition, these techniques are rather insensitive for discriminating tumoral lesions from postoperative abnormal pathologic tissue or necrosis after radiotherapy. This problem, which affects morbidity, has been addressed by special methods such as 18F-fluorodeoxyglucose positron emission tomography (PET), and functional MRI (fMRI) procedures such as MR spectroscopy (MRS), diffusion-weighted imaging (DWI), and PWI (3–5). PET can provide preoperative information of tumor vascularity; however, the spatial resolution is inadequate and the technique is insensitive for demonstrating small lesions (6). To date, only biopsy or surgical resection can provide details on tumor vascularity.

Dynamic susceptibility contrast (DSC) PWI is based on the measurement of the MR signal intensity using a T2*-weighted (T2*W) sequence during the first pass of a bolus of a paramagnetic contrast agent. PWI provides noninvasive physiologic measurements of tumor vascularity and relative cerebral blood volume (rCBV) maps, which can be used to identify and quantify areas of neovascularization (7,8). Vascular proliferation and tumor angiogenesis are the most important factors in the biological behavior of glial tumors (9,10). An increase in the microvascularity and neovascularity of these lesions leads to increased rCBV ratios. Various studies have reported that CBV can demonstrate tumor vascularity both qualitatively and quantitatively. PWI potentially can be used for tumor grading, demonstrating the optimum tumoral area before stereotactic biopsy, discriminating radiation necrosis from tumoral lesions, and assessing the response of the tumor to treatment (7). Making a differential diagnosis of various intracranial lesions preoperatively, and grading glial tumors histopathologically are very important in terms of man-

[1]Department of Radiology, Uludag University Medical School, Bursa, Turkey.
[2]Department of Radiology, Bursa State Hospital, Bursa, Turkey.
[3]Department of Cardiovascular Surgery, Bursa State Hospital, Bursa, Turkey.
*Address reprint requests to: B.H., Department of Radiology, Uludag University School of Medicine, Gorukle, Bursa, Turkey. E-mail: bhakyemez@uludag.edu.tr
Received September 30, 2005; Accepted June 30, 2006.
DOI 10.1002/jmri.20707
Published online 6 September 2006 in Wiley InterScience (www.interscience.wiley.com).

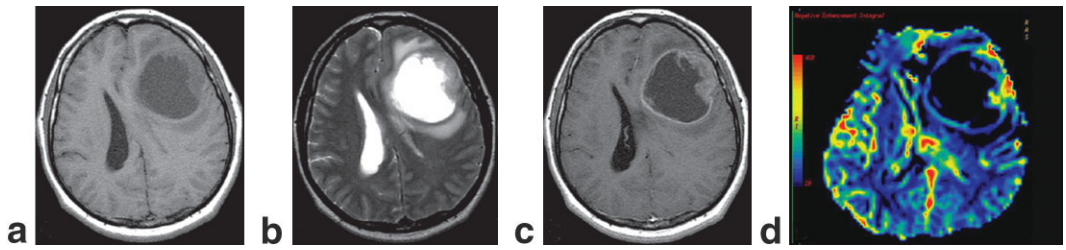

Figure 1. Glioblastoma (grade IV) in a 35-year-old man. Conventional T1W (**a**), T2W (**b**), and postcontrast T1W (**c**) MR images show a left frontal lobe localized lesion that has marked contrast enhancement at the periphery and is surrounded by mild edema. On the CBV image (**d**) there is a high-color-coded area, especially at the lateral site of the lesion, demonstrating hypervascularity. The rCBV ratio of the lesion was 5.59.

agement, prognosis, and monitoring of treatment (11–13). Increased tumor vascularity, however, is not synonymous with malignancy. There are several intracranial extraaxial neoplasms (e.g., meningioma and choroid plexus papilloma) that can be highly vascular but rather benign in terms of biological behavior (14). Although recent PWI studies have focused mostly on glial tumor grading, a limited number of studies about the differential diagnosis of various intracranial tumors have been published (15–27).

In this study our purpose was to investigate the role of PWI, in one of the largest series in the literature, by using rCBV ratios in the differential diagnosis of various intracranial space-occupying lesions.

MATERIALS AND METHODS

Patients

This study was conducted between September 2002 and November 2004, and included 105 patients with lesions (67 males and 38 females, age = 1–77 years, mean = 49.7 ± 17.5 years). The distribution of the lesions was as follows: high-grade glioma (N = 26), low-grade glioma (N = 11), meninigoma (N = 23), metastasis (N = 25), hemangioblastoma (N = 6), bacterial pyogenic abscess (N = 4), schwannoma (N = 5), primary lymphoma of central nervous system (CNS, N = 5). Metastatic lesions originated from the lung (N = 16), breast (N = 7), and kidney (N = 2). Intracranial lesions other than metastatic lesions were diagnosed histopathologically. Sixteen patients with metastatic lesions had undergone surgery and were diagnosed histopathologically. Patients with metastatic lesions had not undergone surgery but had received radiotherapy or chemotherapy. Informed consent was obtained from all subjects according to the guidelines of the institutional review board.

Conventional and PWI Protocols

The examinations were performed with a 1.5-T scanner (Signa LX, GE Medical Systems, Milwaukee, WI, USA). We acquired images using our standard protocol for assessing intracranial lesions. With conventional MRI in the axial plane, T1-weighted (T1W) images (TR/TE = 600/14 msec), T2-weighted (T2W) images (TR/TE = 5400/99 msec) and fluid-attenuated inversion recovery (FLAIR) images (TR/TE/TI = 9000/110/2100 msec) were obtained. Cerebral PWI was performed with a first-pass contrast-enhanced T2*W single-shot gradient-echo echo-planar sequence using a rapid bolus (5 mL/second) of 0.2 mmol/kg of MRI contrast material through an 18- or 20-gauge IV line. The parameters of the sequence were TR/TE = 1972/54 msec, flip angle = 90°, bandwidth = 62.5, field of view (FOV) = 28 × 21 cm, matrix = 96 × 128, section thickness = 6 mm, and section gap = 1.5 mm. A total of 40 images were acquired within 76 seconds (acquisition time). After the PWI, contrast-enhanced T1W images were obtained at the same slice locations and slice thicknesses as the DSC images. The precise algorithm for calculating the rCBV was previously described (28). An rCBV map was derived on a pixel-by-pixel basis from the dynamic image sets. During the first phase of passage by the contrast agent, which was administered rapidly, both the T2* relaxation time and its equivalent T2* signal inten-

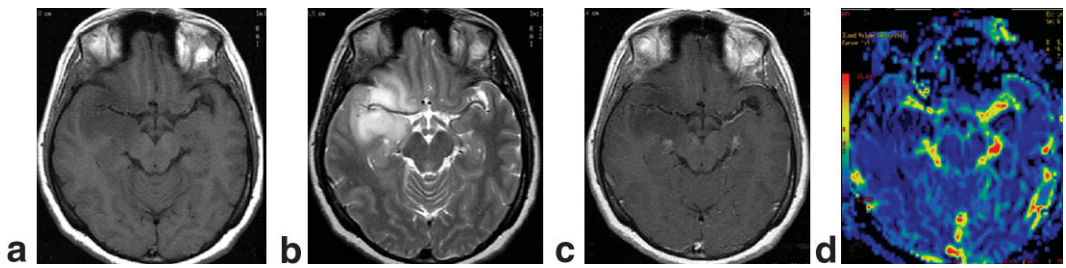

Figure 2. Astrocytoma (grade II) in a 41-year-old man. Conventional T1W (**a**), T2W (**b**), and postcontrast T1W (**c**) MR images show a right temporal lobe localized lesion that extends into the amygdala, temporal uncus, and temporopolar cortex without contrast enhancement. The CBV images (**d**) show no color-coded area in the lesion, indicating hypovascularity. The rCBV ratio of the lesion was 0.83.

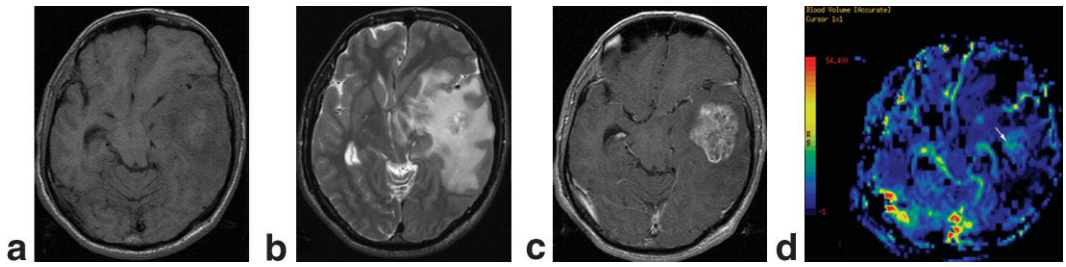

Figure 3. Lung metastasis in a 62-year-old man. Conventional T1W (**a**), T2W (**b**), and postcontrast T1W (**c**) MR images show a left temporal lobe localized lesion that has marked contrast enhancement and severe peritumoral edema. The rCBV image (**d**) shows a color-coded area especially in the central part of the lesion, which indicates hypervascularity (arrow). The rCBV ratio of the lesion was 3.54. [Color figure can be viewed in the online issue, which is available at www.interscience.wiley.com.]

sity had decreased. The change in relaxation rate (ΔR2*) can be calculated based on the signal intensity with the following equation: $\Delta R2^*(t) = \{-\ln (S(t)/S(0))\}/TE$. In this equation TE is the echo time, S(0) is the baseline signal intensity, and S(t) is the pixel intensity at a definite time. ΔR2* is proportional to the concentration of contrast agent in tissue, and CBV is proportional to the area under the curve ΔR2*(t). To estimate the concentration, we fitted a gamma-variate function to the measured ΔR2* curve. Therefore, the recirculation phase of the contrast agent was reduced. rCBV maps were generated as color-scale images by numerical integration of the area under a fitted curve on a pixel-by-pixel basis.

Analyses and Statistics

In the PWI evaluation, the normal white matter of the contralateral hemisphere on the same slice as the lesion was accepted as the standard reference for quantitative analysis. We generated rCBV maps on an Advantage Windows workstation by using the negative enhancement integral program available in the Functool software program (GE Medical Systems). For the color-coded images of CBV, regions of interest (ROIs) of at least 30 mm^2 in size from the lesion with the greatest enhancement and from the normal white matter were used. This procedure was repeated three times for each lesion, and the mean values were calculated. The maximum rCBV ratio within the lesion was calculated according to the equation *of* $rCBV_{ratio} = rCBV_{lesion}/rCBV_{contralateral\ white\ matter}$. We compared the rCBV measurements of the mass lesions with the Mann-Whitney U-test. The rCBV ratios are presented on the basis of the average and standard deviation (SD). A *P*-value less than 0.05 was regarded as statistically significant difference. Statistical analysis was performed using SPSS version 10.0 for Windows (SPSS Inc., Chicago, IL, USA).

RESULT

Conventional Imaging Findings

Glioma

While most of the high-grade gliomas (23/26) enhanced moderately or extensively following contrast administration, in three patients minimal enhancement was demonstrated (Fig. 1). Low-grade gliomas showed moderate (2/11) or minimal/absent (9/11) contrast enhancement (Fig. 2). Cystic or necrotic areas were present in all of the high-grade gliomas except two, and in one low-grade glioma.

Metastasis

Twenty-three of the metastatic lesions showed moderate or severe contrast enhancement, and mild contrast enhancement was observed in two patients. A cystic or necrotic appearance was present in 17 patients. Twenty patients had moderate or severe edema, and the other patients had mild edema (Fig. 3).

Lymphoma

On the postcontrast images, peripherally located, prominent contrast enhancement was present in five

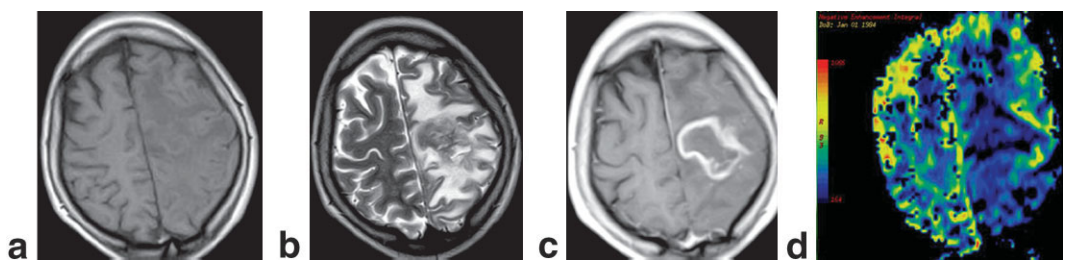

Figure 4. Primary B-cell lymphoma in a 28-year-old man. Conventional T1W (**a**), T2W (**b**), and postcontrast T1W (**c**) images show a left parietal lobe localized lesion with ring-shaped contrast enhancement. The CBV image (**d**) shows hypovascularity of the areas that show contrast enhancement on conventional images. The rCBV ratio was 0.92. The results discriminate lymphoma from cystic metastases and glioma. [Color figure can be viewed in the online issue, which is available at www.interscience.wiley.com.]

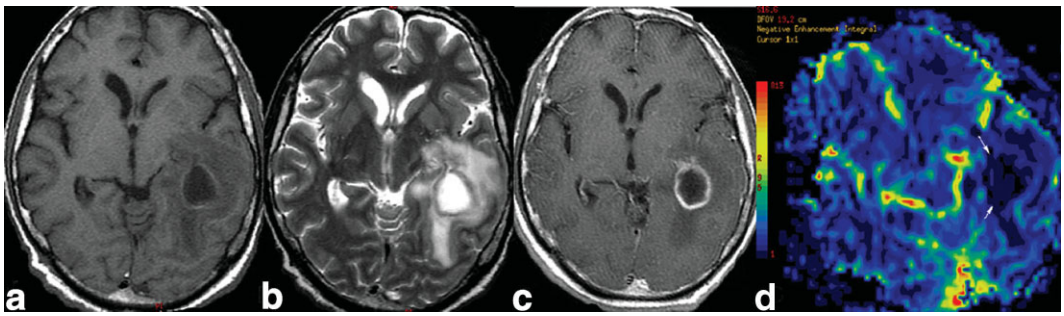

Figure 5. Abscess in a 29-year-old man. Conventional T1W (**a**), T2W (**b**), and postcontrast T1W (**c**) MR images show a left temporal lobe localized lesion that has ring-shaped contrast enhancement and is surrounded by severe edema. The rCBV image (**d**) shows no color-coded area in the sites that enhanced with contrast material on conventional images (arrow). The rCBV ratio of the lesion was 0.62. [Color figure can be viewed in the online issue, which is available at www.interscience.wiley.com.]

out the lymphoma cases, and there was severe edema around the lesions (Fig. 4).

Abscess

Severe edema accompanying ring-shaped contrast enhancement was depicted in all of the lesions (Fig. 5).

Meningioma

All meningiomas enhanced extensively on the postcontrast images (homogeneous $N = 15$; heterogeneous $N = 8$). There were cystic areas in three lesions. Moderate or severe edema was present in eight cases. In other cases, no edema was seen (Figs. 6 and 7).

Schwannoma

On the postcontrast images there was pronounced contrast enhancement in schwannomas localized in the cerebellopontin angle. Three lesions were homogenous, and the others had central cystic necrosis areas (Fig. 8).

Hemangioblastoma

Two out of six hemangioblastomas were solid. The remaining four were cystic, and showed high contrast enhancement at their nidus on postcontrast images. All lesions were infratentorially localized (Fig. 9).

PWI Findings

The rCBV measurements of all lesions are summarized in Table 1. Table 2 summarizes the ranges, means, and SDs of the rCBV ratios for each group of lesions. The difference between rCBV ratios of high- and low-grade gliomas was statistically significant ($P < 0.001$). The rCBV ratios of high-grade gliomas were higher than those of abscesses and lymphomas ($P < 0.001$). The mean rCBV ratios of 17 typical meningiomas were calculated as 6.63 ± 2.87, whereas the mean rCBV ratio of six atypical meningiomas was 12.25 ± 4.63 ($P < 0.01$). The rCBV ratios of meningiomas were higher than those of schwannomas. In addition, there was a statistically significant difference between the rCBV ratios of schwannomas and metastases ($P < 0.05$). The rCBV ratios of lung ($N = 16$) and breast ($N = 7$) metastases were not statistically different ($P > 0.05$).

DISCUSSION

Despite recent technological improvements and the availability of conventional MR images of high quality, it is still not possible to differentiate and grade certain lesions preoperatively. PWI, which is based on tissue physiology, provides valuable information about tumoral vascularity. In the light of these considerations, we analyzed the rCBV ratios of 105 intracranial space-occupying lesions in this study, and the results suggest

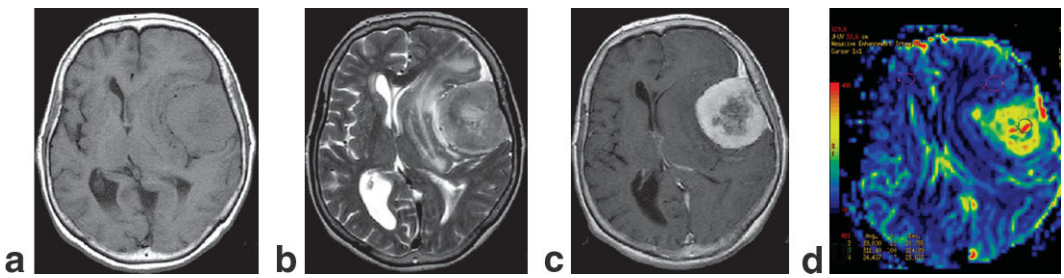

Figure 6. Typical meningioma (grade I) in a 55-year-old woman. Conventional T1W (**a**), T2W (**b**), and postcontrast T1W (**c**) images depict an apparently enhancing extraaxial mass lesion with a necrotic component, apparent peritumoral edema, and mass effect. The color-coded CBV image (**d**) demonstrates pronounced hypervascularity. The intratumoral rCBV ratio was 5.45. [Color figure can be viewed in the online issue, which is available at www.interscience.wiley.com.]

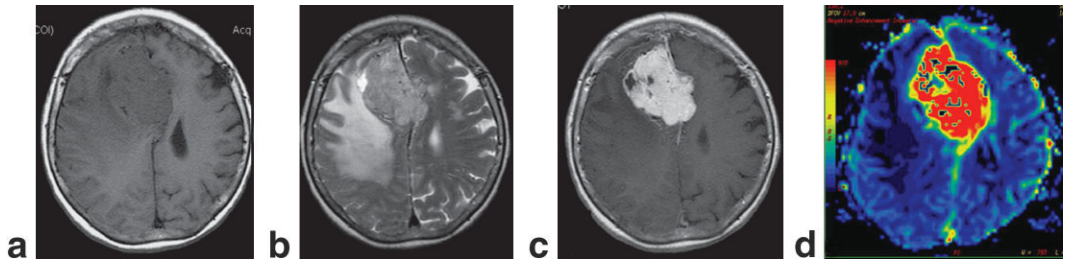

Figure 7. Atypical meningioma (grade II) in a 49-year-old woman. Conventional T1W (**a**), T2W (**b**), and postcontrast T1W (**c**) images depict a strikingly enhancing mass lesion with a necrotic component, apparent peritumoral edema, and mass effect. The color-coded rCBV image (**d**) demonstrates pronounced hypervascularity. The intratumoral rCBV ratio was 14.50. Atypical meningiomas are more vascularized than typical meningiomas. [Color figure can be viewed in the online issue, which is available at www.interscience.wiley.com.]

that PWI is a promising means of differentiating intracranial lesions.

Glioma

On conventional MR images, contrast enhancement of intracranial intraaxial masses is due to destruction of the blood–brain barrier (BBB) rather than hyperplasia or proliferation of blood vessels in the lesion (29–31). Contrast enhancement on PW images is directly related to vascular proliferation (18). Increased vascular proliferation in intraaxial tumors causes neovascularity and increased microvascularity. This condition is one of the most important factors in the grading of lesions, especially gliomas (21). Gliomas are the most common primary malignant tumors of the CNS. Their histopathology varies from low- to high-grade, which is of utmost importance in terms of management, prognosis, and treatment (13,14). Accurate determination of tumor grade is essential for planning optimal treatment strategies. Vascular angiogenesis and proliferation are an important criteria for histopathologic tumoral grading which show biological behavior (13). Several recent studies found statistically significant correlations between tumoral rCBV values and histopathological grades. In our study we also demonstrated that the rCBV ratios of high-grade gliomas (5.76 ± 3.35) were higher than those of low-grade gliomas (1.69 ± 0.52). The rCBV ratios in low-grade gliomas evaluated in our study showed that rCBV was lower or only slightly increased compared to normal brain parenchyma of the contralateral hemisphere.

Meningioma

Meningiomas are extraaxially localized, generally benign lesions, and they account for 15% to 20% of all intracranial tumors. Atypical meningiomas account for 7.2% of all meningiomas, while malignant meningiomas are rare and account for approximately 2.4% (32,33). Malignant and atypical meningiomas are more prone to recurrence, which increases morbidity and mortality. It would be useful to be able to distinguish among benign, malignant, and atypical meningiomas before resection, since it would aid in both surgical and treatment planning (34). Meningiomas are highly vascular tumors that can destroy the whole BBB. For this reason, that have very extensive contrast enhancement on conventional MR images. They are readily identifiable imaging features radiologically. Once they invade the brain parenchyma, they can be misinterpreted as intraaxial tumors invading duramaters (14). Several studies have reported finding meningiomas on PWI. In those studies the rCBV ratios were reported to be higher than that of high-grade gliomas due to high vascularity. Cha et al (14) and Kremer et al (23) obtained rCBV ratios in 12 and nine cases, respectively. In our study we noticed that the rCBV ratios of all 23 meningiomas (8.02 ± 3.89) were higher than those of high-grade gliomas and metastases. Yang et al (35) re-

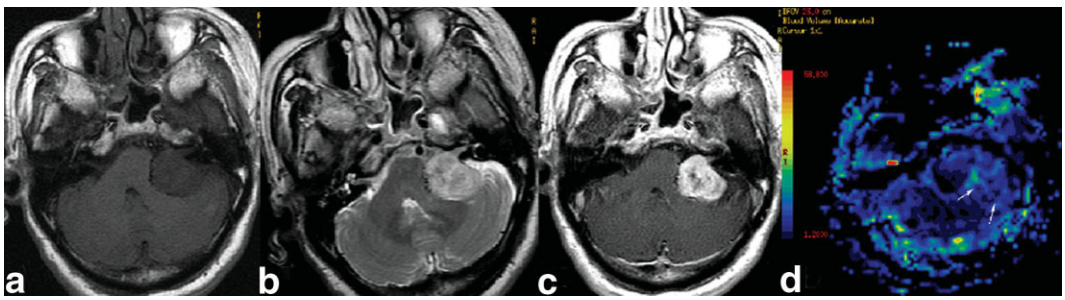

Figure 8. Schwannoma in a 51-year-old woman. Conventional T1W (**a**), T2W (**b**), and postcontrast T1W (**c**) MR images show a remarkable enhancing lesion at the cerebellopontine angle, which extends into the acoustic canal, with areas lacking contrast enhancement showing necrosis. On the CBV image (**d**) there is no color-coded area (in contrast to Fig. 4), which indicates less hypervascularity than meningiomas (arrows). The rCBV ratio of the lesion was 2.45. [Color figure can be viewed in the online issue, which is available at www.interscience.wiley.com.]

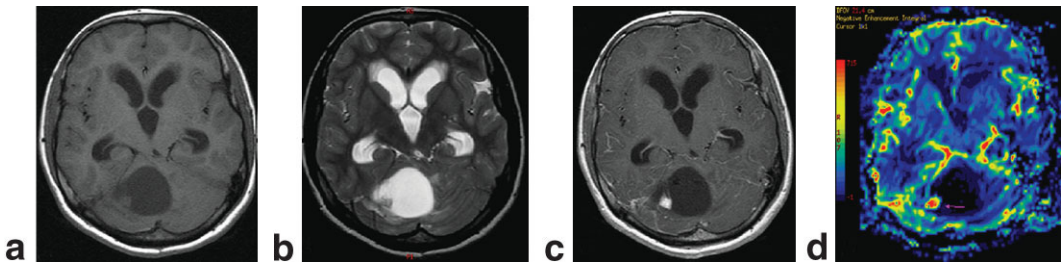

Figure 9. Hemangioblastoma in a 35-year-old man. Conventional T1W (**a**), T2W (**b**), and postcontrast T1W (**c**) MR images show a cystic cerebellar lesion with an apparently enhanced nidus at the periphery and mild edema. The CBV image (**d**) shows a color-coded area especially in the lateral part of the lesion, which shows marked hypervascularity. The rCBV ratio of the lesion was 18.56. [Color figure can be viewed in the online issue, which is available at www.interscience.wiley.com.]

ported that typical and atypical meningiomas can be differentiated from each other, in a study in which perfusion MRI findings of 15 typical and seven atypical meningiomas were correlated with histopathology. In their study the mean rCBV ratio was 8.02 ± 4.74 for typical meningiomas, and 10.50 ± 2.1 for atypical meningiomas (35). In our study the mean rCBV ratio was 6.63 ± 2.87 for 17 typical meningiomas, and 12.25 ± 4.63 for six atypical meningiomas.

Metastasis

Intracranial metastases are the most frequently encountered tumors with high-grade gliomas, and the most frequently-metastasized tumor to the brain is lung cancer (36). It is important to discriminate these tumors from other types, especially high-grade gliomas, in order to establish the treatment protocol and evaluate the prognosis (14). Although conventional MR is very helpful in these cases, it is hard to discriminate primary tumor from metastatic lesion in patients who have a solitary metastasis and whose clinical findings are not obvious (17). Metastatic tumors spread into the CNS via hematogenous routes and induce neovascularization as they grow and expand. Several studies in the literature reported that rCBV ratios are not useful for discrimination (20,23). In our study we also demonstrated that the rCBV ratios of 25 patients with metastasis were not helpful for discriminating these tumors from high-grade gliomas. Previous studies have shown that rCBV ratios of peritumoral edema in patients with metastases are low, whereas they are high in patients with high-grade gliomas, and thus have a high sensitivity for discrimination. In metastases, peritumoral edema represents pure vasogenic edema caused by increased interstitial water due to leaky capillaries. In high-grade gliomas, on the other hand, the peritumoral region represents a variable combination of vasogenic edema and tumor cells infiltrating along the perivascular spaces. There is no neoplastic cell invasion in peritumoral areas of metastatic lesions (14). No statistically significant difference was found between the rCBV values of breast or lung metastases. However, it would be interesting to obtain the rCBV values of various metastatic lesions and to assess the results in larger series, especially those involving hyper- and hypovascular metastases, since rCBV ratios could be helpful in discriminating between the two.

Table 1
The rCBV Ratios for Each Pathologic Group, with Mean and SD, Extreme Values (Range) and Number of Patients Included (*N*) in the Group

Pathologic group (*N* = 105)	rCBV	
	Mean + SD	Range
High-grade glioma (*N* = 26)	5.76 ± 3.35	2.59–18.6
Low-grade glioma (*N* = 11)	1.69 ± 0.51	0.97–2.88
Meningoma (*N* = 23)	8.02 ± 3.89	3.06–16.9
Metastasis (*N* = 25)	5.27 ± 3.22	1.53–15.2
Hemangioblastoma (*N* = 6)	11.36 ± 4.41	6.12–18.5
Abscess (*N* = 4)	0.76 ± 0.12	0.62–0.93
Schwannoma (*N* = 5)	3.23 ± 0.81	2.23–4.45
Lymphoma (*N* = 5)	1.10 ± 0.32	0.78–1.64

Hemangioblastoma

Hemangioblastoma is the most frequent tumor of the posterior fossa in adults after metastasis (36). Some cases are related to von Hippel-Lindau syndrome. They are usually solitary and often localized in the cerebellum; however, they can also be localized in the spinal cord or supratentorial regions (37). A demonstration of hypervascular nidus via angiography is pathognomonic for this tumor (38). Two of our patients had von Hippel-Lindau syndrome. In our study the nidus was hypervascular in all cases with PWI. Cho et al (20) demonstrated that increased rCBV ratios are helpful for differentiating pilocytic astrocytomas from hemangioblastomas, which is not possible with conventional images. In our study we also demonstrated that rCBV ratios were clearly increased and there was a statistically significant difference from all other intracranial masses. We think it could helpful in discriminating hemangioblastoma localized in the posterior fossa from cerebellar metastasis in adults, and from high- and low-grade gliomas in children.

Lymphoma

Lymphomas of the primary central system account for about 6% of all intracranial masses. These lesions are often related to immune suppression syndromes (38,39). It is hard to distinguish these lesions from high-grade gliomas and metastases with conventional MRI. However, accurate diagnosis is very important for

Table 2
Statistical Analysis of Various Intracranial Masses

Lesion	LGG	Meningioma	Metastases	HGB	Abscess	Lymphoma	Schwannoma
HGG	$P < 0.001$	$P < 0.05$	$P > 0.05$	$P < 0.05$	$P < 0.001$	$P < 0.001$	$P < 0.01$
LGG		$P < 0.001$	$P < 0.001$	$P < 0.001$	$P < 0.001$	$P < 0.05$	$P < 0.01$
Meningioma			$P < 0.05$	$P > 0.05$	$P < 0.001$	$P < 0.001$	$P < 0.001$
Metastases				$P < 0.05$	$P < 0.001$	$P < 0.001$	$P < 0.05$
HGB					$P < 0.001$	$P < 0.001$	$P < 0.01$
Abscess						$P > 0.05$	$P < 0.01$
Lymphoma							$P < 0.01$

HGG = high-grade glioma, LGG = low-grade glioma, HGB = hemangioblastoma.

management (14). Unlike other high-grade intracranial neoplasms, lymphoma is treated with combined chemotherapy and radiation therapy without surgery (40). Several previous studies reported that they are less vascular than high-grade gliomas (22,41). Remarkable contrast enhancement on conventional images is due to BBB destruction, and not to neovascularization (14). In our study, lymphomas were hypovascular on PWI, and their rCBV ratios (1.10 ± 0.32) were much lower than those of malignant tumors, especially high-grade gliomas and metastases.

Schwannoma

Schwannomas account for about 6% of all intracranial neoplasms (36). They usually originate from nerve VIII. They can be diagnosed easily with conventional techniques when they are small and localized in the cerebellopontin angle cistern. However, once they reach a large size and the intracanalicular part is not obvious, it may be difficult to discriminate them from meningiomas and metastases localized at the cerebellopontin angle system (42). In our study we demonstrated that rCBV ratios of schwannomas (3.23 ± 0.81) were lower than those of meningiomas and metastases. For this reason, PWI could be helpful for discriminating schwannomas from meningiomas or other masses.

Abscess

In recent times there have been much fewer intracranial abscess cases, due to the use of antibiotics (14). Abscess (especially in the capsule phase) can be misdiagnosed as a malignant cystic lesion (43). In some cases it is impossible to discriminate these lesions from cystic glial tumors or cystic metastases with conventional techniques. DWI and proton MRS are useful for making a differential diagnosis. The apparent diffusion coefficient (ADC) value of an abscess is low because of the viscous content, and abscesses are hyperintense on DW images. The ADC value of a cystic brain tumor is higher due to the serous content, and cystic brain tumors are hypointense on DW images (44). Once a brain tumor is infected or has hemorrhagic content, it has the same intensity as an abscess on DWI and is difficult to diagnosis (45,46). In the literature there are few studies about PWI findings of abscess (24,47). In the experimental setting, brain abscesses have been shown to have relatively high amounts of mature collagen and decreased neovascularity (48). On a theoretical basis, such histologic features should be associated with low capillary density and rCBV, which may serve explain the lower rCBV ratios found in abscesses (47). In our study, rCBV ratios obtained from the capsular portions of the bacterial pyogenic abscesses in four cases were significantly lower than those of malignant cystic tumors when compared with normal white matter. The CBV images of all of the high-grade gliomas and metastases demonstrated various degrees of hypervascularization and markedly increased CBV ratios.

In conclusion, the rCBV ratios of lesions are very helpful for discriminating intracranial space-occupying lesions by demonstrating lesion vascularity. The current results suggest that it is helpful for discriminating between 1) high- and low-grade gliomas, 2) hemangioblastoma and other intracranial posterior fossa masses (because the nidus is highly vascular and the rCBV ratio is very high), 3) ring-enhancing abscess and necrotic high-grade glioma and metastasis, 4) schwannoma and meningioma located in the posterior fossa, 5) lymphoma and high-grade glioma and metastasis, and 6) typical and atypical meningiomas.

REFERENCES

1. Petrella JR, Provenzale JM. MR perfusion imaging of the brain: techniques and applications. AJR Am J Roentgenol 2000;175:207–219.
2. Felix R, Schorner W, Laniado M, et al. Brain tumors: MR imaging with gadolinium-DTPA. Radiology 1985;156:681–688.
3. Wong JC, Provenzale JM, Petrella JR. Perfusion MR imaging of brain neoplasms. AJR Am J Roentgenol 2000; 174:1147–1157.
4. Poptani H, Gupta RK, Roy R, Pandey R, Jain VK, Chhabra DK. Characterization of intracranial mass lesions with in vivo proton MR spectroscopy. AJNR Am J Neuroradiol 1995;16:1593–1603.
5. Burnetti A, Alfano B, Soricelli A, et al. Functional characterization of brain tumors: an overview of the potential clinical value. Nucl Med Biol 1996;23:699–715.
6. Kahn D, Follett KA, Bushnell DL, et al. Diagnosis of recurrent brain tumor: value of 201Tl-SPECT and ^{18}F-fluorodeoxyglucose PET. AJR Am J Roentgenol 1994;163:1459–1465.
7. Lev M, Rosen B. Clinical applications of intracranial perfusion MR imaging. Neuroimaging Clin N Am 1999;9:309–331.
8. Rosen BR, Belliveau JW, Vevea JM, et al. Perfusion imaging with NMR contrast agents. Magn Reson Med 1990;14:249–265.
9. Brem S. The role of vascular proliferation in the growth of brain tumors. Clin Neurosurg 1976; 23:440–453.
10. Zagzag D, Friedlander DR, Dosik J, et al. Tenascin-C expression in angiogenic vessels of human astrocytomas and by human endothelial cells in vitro. Cancer Res 1996;56:182–189.
11. Aronen HJ, Gazit IE, Louis DN, et al. Cerebral blood volume maps of gliomas: comparison with tumor grade and histologic findings. Radiology 1994;191:41–51.
12. Le Bihan D, Douek M, Arygropoulou M, et al. Diffusion and perfusion magnetic resonance imaging in brain tumors. Top Magn Reson Imaging 1993;5:25–31.

13. Bagley LJ, Grossman RI, Judy KD, et al. Gliomas: correlation of magnetic susceptibility artifact with histologic grade. Radiology 1997;202:511–516.
14. Cha S, Knopp EA, Johnson G, Wetzel SG, Litt AW, Zagzag D. Intracranial mass lesions: dynamic contrast-enhanced susceptibility-weighted echo-planar perfusion MR imaging. Radiology 2002; 223:11–29.
15. Knopp EA, Cha S, Johnson G, Mazumdar A, et al. Glial neoplasms: dynamic contrast-enhanced T2*-weighted MR imaging. Radiology 1999;211:791–798.
16. Siegal T, Rubinstein R, Tzuk-Shina T, Gomori JM. Utility of relative cerebral blood volume mapping derived from perfusion magnetic resonance imaging in the routine follow up of brain tumors. Neurosurgery 1997;86:22–27.
17. Law M, Cha S, Knopp EA, et al. High-grade gliomas and solitary metastases: differentiation by using perfusion and proton spectroscopic MR imaging. Radiology 2002;222:715–721.
18. Sugahara T, Korogi Y, Kochi M, et al. Correlation of MR imaging-determined cerebral blood volume maps with histologic and angiographic determination of vascularity of gliomas. AJR Am J Roentgenol 1998;171:1479–1486.
19. Lee SJ, Kim JH, Kim YM, et al. Perfusion MR imaging in gliomas: comparison with histologic tumor grade. Korean J Radiol 2001;2: 1–7.
20. Cho KS, Na GD, Ryoo WJ, et al. Perfusion MR imaging: clinical utility for the differential diagnosis of various brain tumors. Korean J Radiol 2002;3:171–179.
21. Sugahara T, Korogi Y, Tomiguchi S, et al. Posttherapeutic intraaxial brain tumor: the value of perfusion-sensitive contrast-enhanced MR imaging for differentiating tumor recurrence from nonneoplastic contrast-enhancing tissue. AJNR Am J Neuroradiol 2000;21:901–909.
22. Hartmann M, Heiland S, Harting I, et al. Distinguishing of primary cerebral lymphoma from high-grade glioma with perfusion-weighted magnetic resonance imaging. Neurosci Lett 2003;27;338: 119–122.
23. Kremer S, Grand S, Remy C, et al. Cerebral blood volume mapping by MR imaging in the initial evaluation of brain tumors. Neuroradiol 2002;29:105–113.
24. Chan JH, Tsui EY, Chau LF, et al. Discrimination of an infected brain tumor from a cerebral abscess by combined MR perfusion and diffusion imaging. Comput Med Imaging Graph 2002;26:19–23.
25. Provenzale JM, Wang GR, Brenner T, Petrella JR, Sorensen AG. Comparison of permeability in high-grade and low-grade brain tumors using dynamic susceptibility contrast MR imaging. AJR Am J Roentgenol 2002;178:711–716.
26. Lam WW, Chan KW, Wong WL, Poon WS, Metreweli C. Pre-operative grading of intracranial glioma. Acta Radiol 2001;4:548–554.
27. Shin JH, Lee HK, Kwun BD, et al. Using relative cerebral blood flow and volume to evaluate the histopathologic grade of cerebral gliomas: preliminary results. AJR Am J Roentgenol 2002;179:783–789.
28. Hakyemez B, Erdogan C, Ercan I, Ergin N, Uysal S, Atahan S. Distinguishing high-grade glioma from low-grade glioma with perfusion-weighted magnetic resonance imaging. Clin Radiol 2005;60: 493–502.
29. Johnson PC, Hunt SJ, Drayer BP. Human cerebral gliomas: correlation of postmortem MR imaging and neuropathologic findings. Radiology 1988;166:823-827.
30. Brasch RC, Weinmann HJ, Wesbey GE. Contrast-enhanced NMR imaging: animal studies using gadolinium-DTPA complex. AJR Am J Roentgenol 1984;8:204–207.
31. Leon S, Folkerth R, Black P. Microvessel density is a prognostic indicator for patients with astroglial brain tumors. Cancer 1996; 77:362–372.
32. Verheggen R, Finkenstaedt M, Bockermann V, Markakis E. Atypical and malignant meningiomas: evaluation of different radiological criteria based on CT and MRI. Acta Neurochir 1996;65:66–69.
33. Mahmood A, Caccamo DV, Tomecek FJ, Malik GM. Atypical and malignant meningiomas: a clinicopathological review. Neurosurgery 1993;33:955–963.
34. Ayerbe J, Lobato RD, de la Cruz J, et al. Risk factors predicting recurrence in patients operated on for intracranial meningioma: a multivariate analysis. Acta Neurochir (Wien) 1999;141:921–932.
35. Yang S, Law M, Zagzag D, et al. Dynamic contrast-enhanced perfusion MR imaging measurements of endothelial permeability: differentiation between atypical and typical meningiomas. AJNR Am J Neuroradiol 2003;24:1554–1559.
36. Black P. Brain tumors. N Engl J Med 1991;324:1555–1564.
37. Lee SR, Sanches J, Mark AS, Dillon WP, Norman D, Newton TH. Posterior fossa hemangioblastomas: MR imaging. Radiology 1989; 171:463–468.
38. Ho VB, Smirniotopoulos JG, Murphy FM, Rushing EJ. Radiologic-pathologic correlation: hemangioblastoma. AJNR Am J Neuroradiol 1992;13:1343–1352.
39. Schabet M. Epidemiology of primary CNS lymphoma. J Neurooncol 1999;43:199–201.
40. Reni M, Ferreri AJ, Garancini MP, Villa E. Therapeutic management of primary central nervous system lymphoma in immunocompetent patients: results of a critical review of the literature. Ann Oncol 1997;8:227–234.
41. Sugahara T, Korogi Y, Shigematsu Y, et al. Perfusion-sensitive MRI of cerebral lymphomas: a preliminary report. J Comput Assist Tomogr 1999;23:232–237.
42. Press GA, Hesselink JR. MR imaging of cerebellopontine angle and internal auditory canal lesions at 1.5 T. AJNR Am J Neuroradiol 1988;9:241–251.
43. Haimes AB, Zimmerman RD, Morgello S, et al. MR imaging of brain abscess. AJR Am J Roentgenol 1989;152:1073–1077.
44. Kim YJ, Chang KH, Song IC, et al. Brain abscess and necrotic or cystic brain tumor: Discrimination with signal intensity on diffusion-weighted MR imaging. AJNR Am J Neuroradiol 1998;171:1487–1490.
45. Hartmann M, Jansen O, Heiland S, Sommer C, Munkel K, Sartor K. Restricted diffusion within ring enhancement is not pathognomonic for brain abscess. AJNR Am J Neuroradiol 2001;22:1738–1742.
46. Ernst TM, Chang L, Witt MD, et al. Cerebral toxoplasmosis and lymphoma in AIDS: perfusion MR imaging experience in 13 patients. Radiology 1998;208:663–669.
47. Holmes MT, Petrella JR, Provenzale JM. Distinction between cerebral abscesses and high-grade neoplasms by dynamic susceptibility contrast perfusion MRI. AJR Am J Roentgenol 2004; 183:1247–1252.
48. Britt RH, Enzmann DR, Yeager AS. Neuropathological and computerized tomographic findings in experimental brain abscess. J Neurosurg 1981;55:590–603.